Mechanics of fiber-reinforced hyperelastic solids
Report for the W. M. Keck Institute of Space Studies

Francisco Lopez Jimenez

September 30, 2010

Abstract

Recent designs for deployable space structures include elements that can be folded to high curvatures and recover elastically. A type of material proposed for such hinges is fiber composites with a soft silicone matrix. This research focuses on the characterization of this type of composites. Their mechanical properties during folding have been studied experimentally, revealing a highly non-linear moment-curvature relationship and stress softening, due to micro-damage. The micromechanics of the problem have also been studied numerically, with a finite element model that takes into account the arrangement of the fibers. The model predicts most of the features observed experimentally, including the microbuckling that reduces fiber strain during folding. The model overestimates the material stiffness, due to its inability to model the damage taking place in the material. Current efforts are focused on modeling this damage process. In order to do so, the tension stiffness transverse to the fibers has been measured. Preliminary results including cohesive elements that delamination show good agreement with the tests.

1 Introduction

Most space structures include elements that are deployed after launch. This has traditionally been achieved with mechanical elements, such as joints, that allow relative motion between parts of the structure. In more recent alternatives, this motion is achieved by elastically straining the structural elements, such as tape springs made of ultra-thin fiber composite materials. Examples of this type of architecture can be seen in Figure 1.

These structures are lightweight, have a low cost, and are simpler than the traditional mechanically actuated alternatives. This makes them particularly interesting for small satellite missions. The main limitation on the further improvement of their packing ratio is the failure curvature of the material. New designs have appeared in recent years for structures requiring hinges that can achieve high curvatures and recover elastically [6, 9], or reflectors made with superelastic materials, which could be folded in a much more compact way. Possible materials to be used in those structures are composites in which the fibers are bonded by a very soft and flexible matrix, such as silicones and elastomers. Such materials can be folded to a much higher curvature than composites made with traditional stiff matrix. This new type of composites has already been used to build models showing exceptional folding capabilities [2, 5] (Figure 2). However, the mechanics of this new type of material is not properly understood yet.

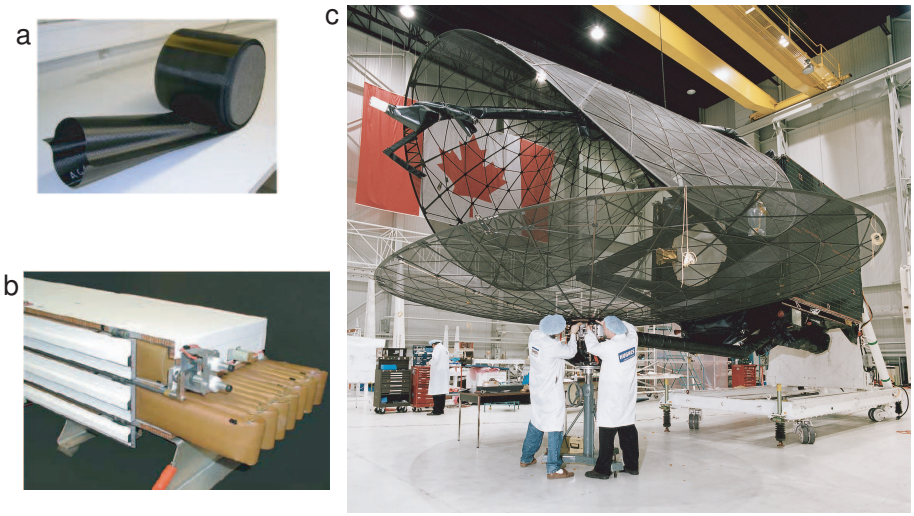

Figure 1: Examples of deployable space structures: (a) DLR-CFRP boom, German Aerospace Center [4], (b) Northrop Grumman Astro Aerospace Flattenable Foldable Tubes for the Mars Express [1] and (c) Boeing springback reflectors on the Mobile Satellite System [11].

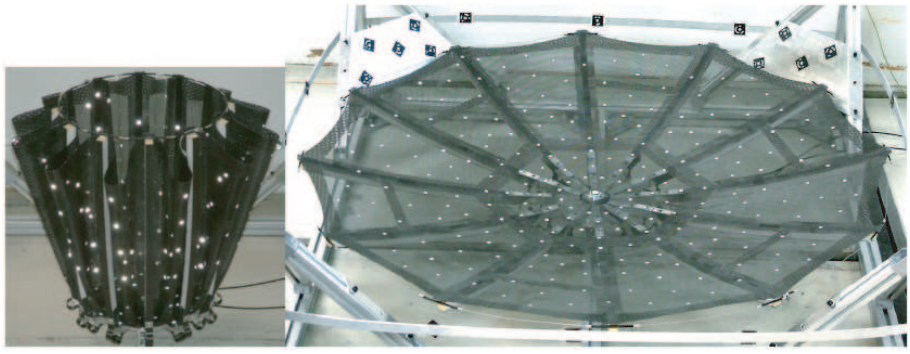

Figure 2: SMART demonstrator with an umbrella-like deployment scheme, folded and deployed [2].

The aim of this research is to characterize the mechanical behavior of fiber composites with silicone matrix, and to create the analytical and numerical tools that are necessary to incorporate this kind of material in a real design. In particular, the material shows a highly nonlinear moment-curvature relationship when folded. A finite element analysis of the micromechanics of the fibers show that the reason is microbuckling of the fibers in the compressive side. The numerical model used takes into consideration the fiber arrangement observed in the real material. This allows to study the effect of a the traditional assumption of a regular lattice.

Another difference with standard composite materials is the presence of strain softening, also known as Mullins effect. This is a noncritical damage process that reduces the stiffness of the material when it is subjected to cyclic loading, until it reaches an equilibrium state. A new finite element model for the transverse loading of the material is currently being developed, in which the softening is modeled as the effect of debonding between the fibers and the matrix.

2 Folding experiments

The fibers used are HTS40-12K, produced by TohoTenax [12]. They were provided by Itochu Corporation, which is responsible for the uniaxial tow spreading. The matrix used is CF19-2615, produced by NuSil Technologies [8]. It is a two part, optically clear silicone. It cures for 30 minutes at 150 °C. The properties of both materials can be seen in Table 1.

Fiber properties	
Diameter	7 μm
Tensile modulus	240 GPa
Density	1.77 g/cm^3
Matrix properties	
Viscosity (part A)	1300 mPa s
Viscosity (part B)	800 mPa s
Density	0.96 g/cm^3
Typical tensile modulus	0.8 MPa
Typical elongation	100%

Table 1: Material properties

In order to observe the material in folded configuration, several initially flat specimens were held at a 90° kink angle, with a radius of curvature of approximately 2 mm. Figure 3 shows the tension and compression side of specimens with 30% fiber volume fraction. Micro buckling can be observed in both cases, although it is more regular and noticeable in the case with lower volume fraction. The buckles appear in both the compression and tension sides, although the amplitude is higher in the compressed fibers. The simulation results agree with this experimental observation. The existence of buckled fibers on the tension side is typical of very thin composites, and does not happen in the case of thicker specimens.

The moment-curvature relationship of the material was calculated for two different volume fractions, 30% and 55%. The response is highly nonlinear, with the stiffness decreasing greatly after buckling takes place. The tests were performed at three different speeds: 0.25, 0.5 and 1 mm/min of vertical displacement (note that a linear vertical displacement does not translate into linear increase in curvature). No significant difference was found between them, and rate dependence effects are therefore neglected.

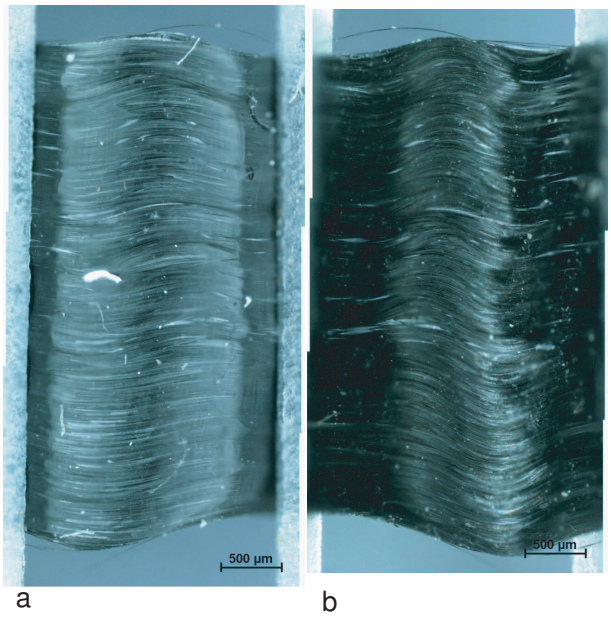

Figure 3: Specimen folded 90° with a 2 mm radius and 30% volume fraction: (a) tension side and (b) compression side

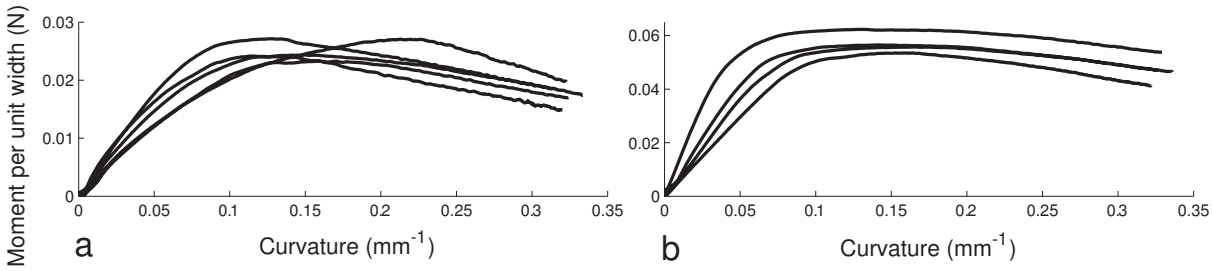

Figure 4: Moment vs. curvature relationship: for experiments with (a) 55% volume fraction and (b) 30% volume fraction. The results show the first test performed on each sample.

If more than one loading-unloading cycle is applied, the specimens show strain induced stress softening, also known as Mullins effect. Figure 5 shows the moment-curvature relationship obtained from a test with a single specimen. A flat specimen was folded in three sets of four cycles, with increasing maximum curvature: 0.22, 0.30 and 0.36 mm^{-1}. The stiffness decreased after each cycle, the difference being higher for the first cycle that reached a given maximum curvature. The same specimen was tested again 24 hours after the first test. The damage was not recovered, and the stiffness was the same as at the end of the previous test. Both the permanent loss of stiffness and the cycle hysteresis are less pronounced in the specimens with lower volume fraction. This agrees with the typical behavior of particle reinforced rubbers.

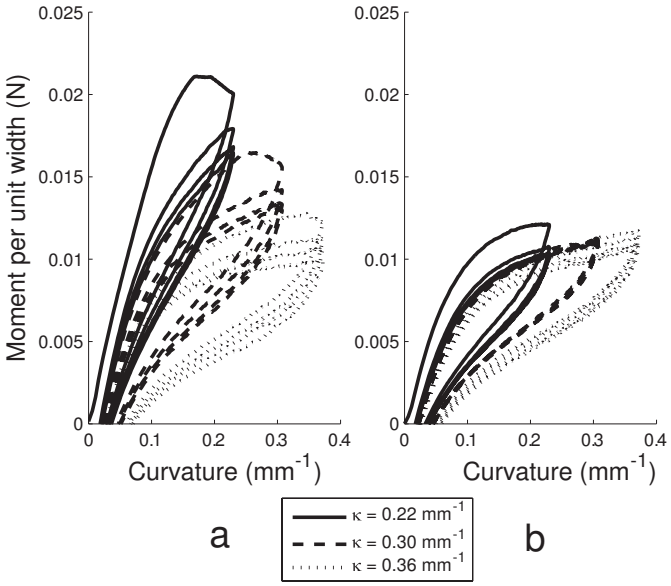

Figure 5: Moment vs. curvature relationship showing Mullins effect. Volume fraction 55%.

3 Folding simulation

A micromechanical finite element model has been set up in the finite element package ABAQUS/Standard. The material is modelled as an elastic continuum, with nonlinear geometry. Both matrix and fibers are modeled with 3D solid elements. The fibers have been modeled as a linear elastic material. The matrix has been modeled using the hyperelastic potential provided by Gent [3], which was implemented in ABAQUS using the user subroutine UHYPER.

In order to reduce the computational cost, only a repeating unit cell of the tow has been modeled. Two different approaches were used to model the fiber arrangement within the unit cell. In the first one, the fibers form an hexagonal grid of cylindrical rods. The distance between the fibers, as well all other geometric properties, depend only on the number of fibers per unit width and the volume fraction, both of them obtained from direct measurements. Although a common idealization, micrographs of the material show that this approach is unrealistic.

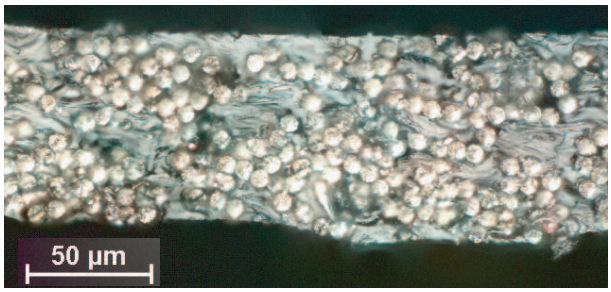

Figure 6: Example picture after stacking process.

Since the fibers are expected to undergo very high deflections, the strain energy in the matrix

will greatly depend on the spacing between fibers. In order to achieve a more realistic unit cell, a reconstruction method based on [10] has been used here. It allocates the fibers randomly within the unit cell, and then allows them to move until the radial distribution function of the model matches that observed experimentally. Figure 7 shows two examples of unit cells obtained with this method.

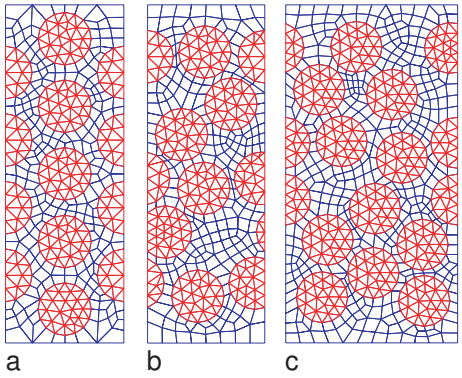

Figure 7: Examples of unit cells with 55% volume fraction: (a) hexagonal pattern, (b) random cell, same width as hexagonal pattern and (c) random cell, 1.5 times width of hexagonal pattern

Figure 8 shows different views of one of the simulations (hexagonal pattern, 55% volume fraction), in which the overall geometric characteristics are present: buckling of the fibres within the plane, large fibre deflections, higher buckle amplitude in the compression side, and very uniform curvature.

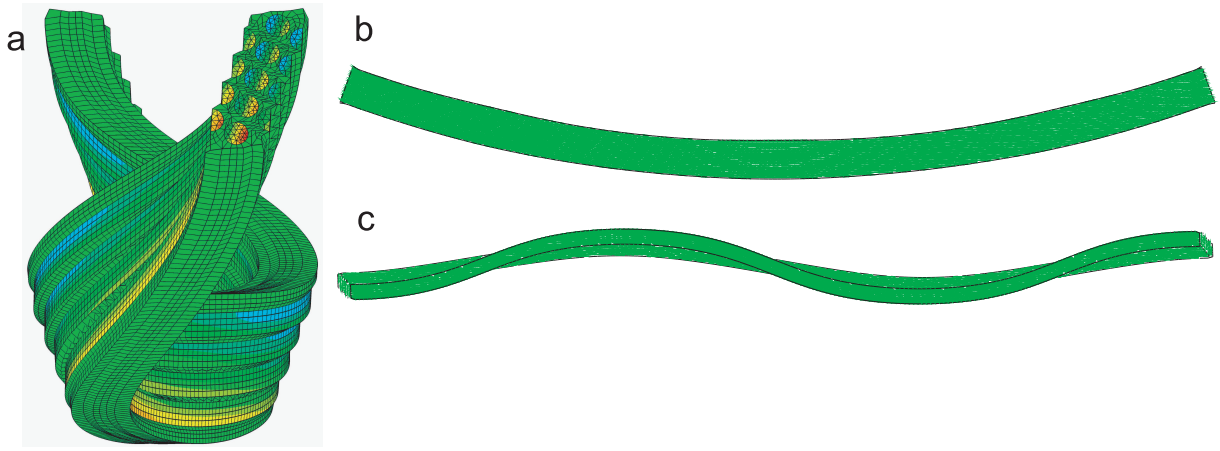

Figure 8: Deflected shape of model with hexagonal fiber arrangement, 55% volume fraction, 1 mm length: (a) front view, (b) side view and (c) top view.

The results of the finite element analysis and the experiments are compared in Figure 9, where the area enveloped by the simulations with random fiber arrangement has been shaded. In the first case of 55% volume fraction the prediction is much stiffer than the real experiments. In the case with 30% volume fraction, the prediction is much closer to the test results. The model provides a

good prediction of the initial stiffness, as well as the curvature marking the transition to the non linear regimen. The post buckled behaviour is again stiffer in the finite element model.

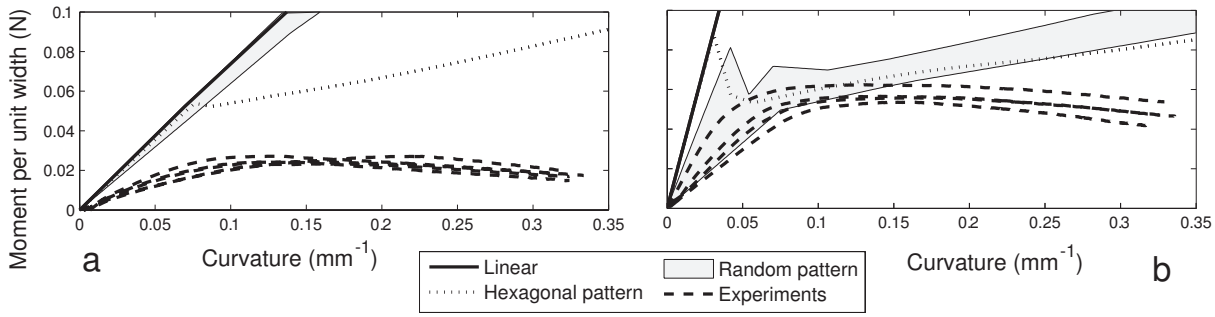

Figure 9: Comparison of moment vs. curvature in simulations and experiments. The plots show the results from the simulation with hexagonal fiber arrangement, the range spanned by the simulations with random unit cell, and five experiments. A linear analysis has been added as a reference. Volume fractions: (a) 55% and (b) 30%

The reason for this discrepancy is the inability of the model to capture the damage taking place in the material. This damage is not only responsible for the Mullins effect, but it is also likely to produce a decrease in stiffness in the material. In order to further improve the model, it is necessary to model and implement this mechanism.

4 Transverse tension experiments

In order to characterize the damage process, the material has also been tested in tension in the direction perpendicular to the fibers. This test creates a much simpler state of stress within the material, which allows for a much simpler analysis.

The experiments show a stress softening very similar to that of the bending experiments. Loading to failure can be observed for the highest strain values.

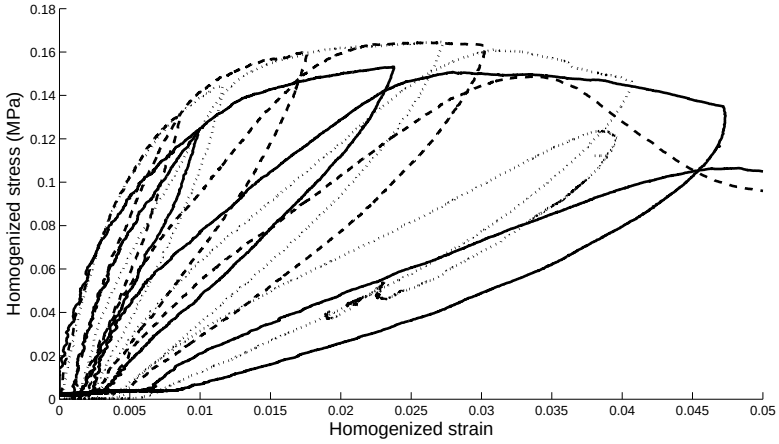

Figure 10: Tension vs. strain in the direction transverse to the fibers. Volume fraction 50%.

5 Transverse tension simulations

Since the material can be modeled as a 2D solid with plane strain, it is now possible to include a much higher number of fibers in the simulations. In this case the matrix and the fibers are connected through cohesive elements, which would be used to model the debonding as the stress increases. The analysis is similar to that performed by Moraleda et al. [7]. Figure 11 shows the strain in the direction of the loading.

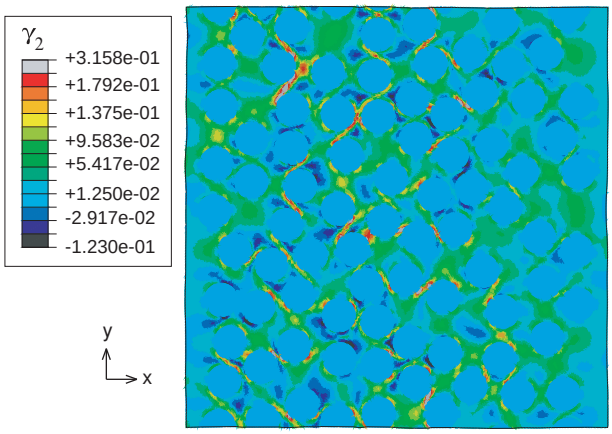

Figure 11: Stress vs. strain transverse to the fibers. Volume fraction 50%. The plot shows the strain concentrations in the matrix.

The properties for the cohesive elements still need to be fitted from the experimental data, but preliminary results show that this modification allows us to capture the overall shape of the curve, in contrast with the case in which the bonding between fibers and matrix is assumed to be perfect. Figure 12 compares the response of the model with and without cohesive elements, and shows the great effect that their inclusion has on the stiffness of the material.

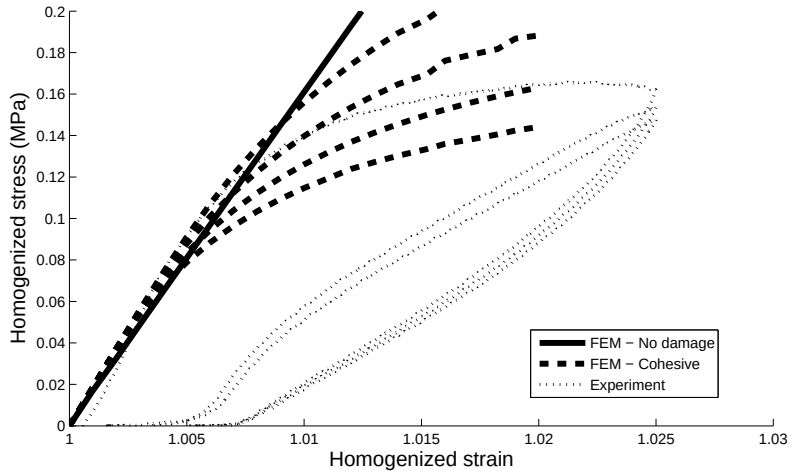

Figure 12: Stress vs. strain transverse to the fibers. The plot shows the response of the finite element model without damage mechanism, the response of the model with cohesive elements for four different values of the critical stress failure, and the results of repeated experiments on a single specimen. Volume fraction 60%.

6 Conclusions

A composite material consisting of unidirectional carbon fibers in a silicone matrix was fabricated and its bending properties were studied experimentally. The material can be folded to very high curvatures, and presents a highly non-linear moment vs. curvature relationship. The experiments also show stress softening similar to Mullins effect.

A finite element model was created in order to study the micro mechanics of the material. It uses a unit cell with two different distributions of the fibres in the model: a regular hexagonal lattice, and a random distribution based on that observed in material micrographs. The cases with 30% volume fraction show good agreement between experiments and simulations, while in the case of 55% volumen fraction the finite element model overestimates the stiffness of the matrix. The difference is likely due to the assumptions of the matrix model, which neglect any failure or damage mechanism.

In order to model this mechanism, the material has been tested in tension in the direction transverse to the fibers. The experiments show Mullins effect, and a progressive softening of the material as the applied load increases. Preliminary results show that including cohesive elements in the model allows to model this softening. Incorporating the cohesive elements into the 3D model used to analyze the folding process would allow further refinement of the model, and capture the softening that takes place in the material as the curvature increases.

Acknowledgements

This study was supported with funding from the W.M. Keck Institute for Space Studies (KISS) at Caltech.

References

[1] D. S. Adams and M. Mobrem. Lenticular jointed antenna deployment anomaly and resolution onbard the mars express spacecraft. *Journal of Spacecraft and Rockets*, 46:403–410, 2009.

[2] L. Datashvili, H. Baier, E. Wehrle, T. Kuhn, and J. Hoffmann. Large shell-membrane space reflectors. In *51st AIAA/ASME/ASCE/AHS/ASC Structures, Structural Dynamics, and Materials Conference*, number AIAA-2010-2504, Orlando, Florida, 2010.

[3] A. N. Gent. Elastic instabilities in rubber. *International Journal of Non-Linear Mechanics*, 40:165 – 175, 2005.

[4] M. Leipold, H. Runge, and C. Sickinger. Large sar membrane antennas with lighweight deployable booms. In *28th ESA Antenna Workshop on Space Antenna Systemas and Technologies*, ESA/ESTEC, 2005.

[5] J. M. Mejia-Ariza, K. Guidanean, T. M. Murphey, and A. Biskner. Mechanical characterization of lgarde elastomeric resin composite materials. In *51st AIAA/ASME/ASCE/AHS/ASC Structures, Structural Dynamics, and Materials Conference*, number AIAA-2010-2701, 2010.

[6] J. M. Mejia-Ariza, E. L. Pollard, and T. W. Murphey. Manufacture and experimental analysis of a concentrated strain based deployable truss structure. In *47th AIAA/ASME/ASCE/AHS/ASC Structures, Structural Dynamics, and Materials Conference*, number AIAA-2006-1686, Newport, Rhode Island, 2006.

[7] J. Moraleda, J. Segurado, and J. Llorca. Effect of interface fracture on the tensile deformation of fiber-reinforced elastomers. *International Journal of Solids and Structures*, 46(9):4287–4297, 2009.

[8] NuSil Silicone Technology. http://www.nusil.com/library/products/CF19-2615P.pdf, March 2007.

[9] F. Rehnmark, M. Pryor, B. Holmes, D. Schaechter, N. Pedreiro, and C. Carrington. Development of a deployable nonmetallic boom for reconfigurable systems of small spacecraft. In *48th AIAA/ASME/ASCE/AHS/ASC Structures, Structural Dynamics, and Materials Conference*, number AIAA-2007-2184, Honolulu, Hawaii, 2007.

[10] M.D. Rintoul and S. Torquato. Reconstruction of the structure of dispersions. *Journal of Colloid and Interface Science*, 186:467–476, 1997.

[11] L. T. Tan and S. Pellegrino. Thin-shell deployable reectors with collapsible stieners: Part 1 approach. *AIAA Journal*, 44:2515–2523, 2006.

[12] Toho Tenax. http://www.tohotenax.com/tenax/en/products/st_property.php, retrieved August 2010.